



This is the accepted manuscript made available via CHORUS. The article has been published as:

Rapid activation of non-oriented mechanophores via shock loading and spallation

Brenden W. Hamilton and Alejandro Strachan

Phys. Rev. Materials **7**, 045601 — Published 18 April 2023

DOI: [10.1103/PhysRevMaterials.7.045601](https://doi.org/10.1103/PhysRevMaterials.7.045601)

Rapid Activation of Non-Oriented Mechanophores via Shock Loading and Spallation

Brenden W. Hamilton, Alejandro Strachan¹

School of Materials Engineering and Birck Nanotechnology Center, Purdue University, West Lafayette, Indiana, 47907 USA

Abstract

Mechanophores, stimuli-responsive molecules that respond chromatically to mechanochemical reactions, are important for understanding the coupling between mechanics and chemistry as well as in engineering applications. However, the atomic-level understanding of their activation originates from gas phase studies or under simple linear elongation forces directly on molecules or polymer chains containing mechanophores. The effect of many-body distortions, pervasive in condensed-phase applications, is not understood. Therefore, we performed large-scale molecular dynamics simulations of a PMMA-spiropyran co-polymer under dynamic mechanical loading and studied the activation of the mechanophore under various conditions from dynamical compression to tension during unloading. Detailed analysis of the all-atom MD trajectories shows that the mechanophore blocks experience significant many-body intra-molecular distortion that can significantly decrease the activation barrier as compared to when deformation rates are slow relative to molecular relaxation timescales. We find that the reactivity of mechanophores under material compression states is governed by many-body effects of intra-molecular torsions, whereas under tension the reactions are governed by tensile stresses.

¹ Corresponding author: strachan@purdue.edu

Introduction

Mechanochemistry, the use of mechanical loads to trigger or influence chemistry, can alter chemical kinetics and decomposition paths in covalent systems [1]. These processes have been widely studied for single molecules and gas-phase systems both experimentally and computationally. [2] Such processes and a general understanding of mechanochemistry are currently applied in industrial applications of various chemicals and materials [3,4]. In general, condensed phase mechanochemistry extends to a broad range of chemical events such as phase transitions in carbon [5], planetary collisions [6–8], and shockwave initiation of high explosives [1,9–12].

Mechanophores are stimuli-responsive materials that undergo chemical reactions, such as isomerization or bond scission, under mechanical stimuli, and this results in a macroscopic, chromatic response, such as color change or fluorescence [4]. The broad range of applications of these materials results in significant interest from both the engineering and basic sciences communities. Hence, significant experimental and computational work has been devoted to increasing our understanding of the governing physics [13–16]. Such a knowledgebase may, in turn, enable the design of mechanophores for a variety of applications such as flexible electronics [17], aerospace, [18] energy infrastructure, [19] catalysis [20], material strengthening [21], and the release of other molecules under controlled conditions [22].

Computational efforts have significantly increased our understanding of mechanochemistry within condensed matter systems. Motivated by experiments using atomic force microscopy to measure covalent bond strength [23], quantum chemistry (QC) and molecular dynamics (MD) methods have proven invaluable in understanding mechanochemical activation and reactions [2,24]. QC and MD methods have been the dominant workhorses for these studies. They helped elucidate the activation processes in mechanophores [13,14,25] and those driving the reduction in strength in knotted and entangled polymer systems [26–29], assess extension and bond breakage in metal-organic junctions under strain [30–32], and explore the stress states associated with protein folding [33]. Often these types of studies, especially those for mechanophores, use special purpose methods such as steered MD [34–38] and the constrained geometries simulate external force (CoGEF) method [39].

These methods are often applied to mechanophores as single truncated systems in the gas phase and neglect a variety of many-body effects incurred in the condensed matter state, especially under shock loading or other high strain rate events. Recent computational studies showed that dynamic strain-induced chemistry in molecular materials can occur at significantly faster rates than under thermodynamically identical, but equilibrium, conditions [9]. Additionally, it has been shown that shockwave-induced shear bands will react orders of magnitude faster than non-sheared sections of the material [10]. The mechanochemical effects have been recently attributed to large intramolecular deformations induced by the high strain rates and significant plastic flow associated with dynamical loading [40–42]. These deformations are significant distortions of a many-body nature; primarily out-of-plane bends and torsional rotations induced in the molecule. Such intramolecular strains can persist well into the timescales of chemical initiation and are known to influence the reaction kinetics and reaction paths [43–47]. The recently developed many-body steered MD method (MBsMD) has been used to show that these complex deformations generally both increase reactivity and alter the 1st step reaction pathways [48]. Specifically, torsional shears applied to the central C-O bond of a spiropyran molecule showed up to a 45% reduction in activation barrier for strain-induced isomerization as compared to simple pulling forces.

Spiropyran, which is used in this work, is a mechano-chromic molecule that undergoes a stress-induced 6π electrocyclic ring-opening reaction via bond scission of the C-O bond, resulting in merocyanine [13]. The activation of these mechanophore reactions is greatly influenced by the properties of the polymer system in which it is incorporated [49]. Conversely, independent of the polymer system, be it glassy or elastomeric, the external forces resolved along the reaction coordinate of the mechanophore must drive the strain energy above a threshold value to induce reaction [50,51]. The activation of these materials can be strain rate-dependent [52], and at slow strain rates, such as in a tensile test, the deformation is distributed rather uniformly throughout the material. Under these conditions, systems typically need to approach macroscopic material failure to induce significant activation of the mechanophore. This is more easily achieved in chains/mechanophores aligned with the macroscopic pulling direction where the macroscopic applied force couples better to the action of elongating the mechanophore. Additionally, compression experiments in Poly(methyl methacrylate) (PMMA) with spiropyran mechanophores showed that the highest levels of activation were localized where Poisson effects maximize the tensile stresses in the lateral directions [13,53] and material experiences a high deviatoric state.

Activation can be greatly influenced by the various environmental factors that affect chain mobility [54]. In general, the response of the mechanophore in condensed matter systems can be greatly influenced by the complex dynamics of polymer chains under dynamic loading, which become increasingly more complex under shock loading [55]. Here, we use dynamical compression and expansion, with timescales much shorter than those associated with chain re-alignment, to study spiropyran activation. Our results show the significance of many-body molecular distortions on activation and the need to consider more than simple elongation forces when studying mechanophore reactions, as well as condensed matter chemistry in general.

For mechanophores embedded in an amorphous polymer system, not all local stresses will be uniaxial and aligned with the active bond. Resolved shears, local collisions, entanglements, and crosslinks can result in some measure of a many-body strain such as out-of-plane bends or torsional rotations. Here we utilize reactive MD simulations of shock loading on a spiropyran-PMMA system in which the sample geometry is designed to go through a progression of compressive and tensile loads that can then induce spall and failure. Shock loading is used as it is known to induce a wide range of many-body strains and rapid local deformations within condensed matter systems [10,40,55]. We show that these loads induce a variety of many-body deformations in the spiropyran block of the chains and that both compression and tension lead to rapid activation. This is compared to a compression-only baseline result. The many-body deformation (strain) and complex stress-velocity states of the activated mechanophores is assessed.

Methods

Simulations are conducted using all-atom MD via the LAMMPS software [56]. The ReaxFF reactive forcefield was used with the ReaxFF-LG parametrization [57] that has been previously used to explore polymer crosslinking [58], graphitization of carbon [59], and reactions in energetic materials, including at high pressures [60,61]. A mechanophore system (MP) consisting of a copolymer of PMMA and spiropyran was built using PolymerModeler [62], an open, online tool available on nanoHUB. The systems are built as PMMA/indolinobenzospiropyran copolymers with the spiropyran as the central monomer block with 40 PMMA monomers on either end (81

monomers total per chain). Using a continuous configurational bias Monte Carlo method [63], we built an initial condensed matter system with 625 chains for a total of 920,000 atoms.

The MP system was initially relaxed using the nonreactive Dreiding forcefield [64] at 800 K in a fully periodic system keeping a 4:1:1 ratio between cell parameters under isobaric, isothermal (NPT) conditions for 100 ps. The system was then cooled to 300 K with a cooling rate of 100 K/ns, at ambient pressure, forcing the cell aspect ratio to remain the same. The glass transition obtained from these simulations, 450 K, was comparable to pure PMMA under the same conditions [65].

Using the reactive force field ReaxFF, which is well parametrized for high-pressure applications [1,9,60,66–72], the 300 K structure was divided into projectile and target sections, see Figure 1, to enable dynamical loading simulations via high-velocity impacts. Two gaps were introduced in the system, by deleting whole chains whose centers of mass fall within a predetermined region, along the long cell direction. The first gap is at the cell boundary to break periodicity, and the second at 1/3 distance into the system. This results in two slabs, 15 nm and 32.5 nm in length, separated by a 10 nm gap, as shown in Figure 1. The large slab contains 364 chains and the small one 148 chains for a final total of 512 total chains and 753,664 atoms. The system was then thermalized for 50ps to allow for surface relaxation.

Ballistic impact simulations [73] were performed with impact velocities ranging from 2.0 to 4.0 km/s. Two distinct systems were used. In the “two-slab system” as shown in Figure 1, slabs were initialized with impact velocities of equal and opposite vectors, where the collision creates two shockwaves of equal strength propagating in opposite directions into the “flyer” and “target”. An example LAMMPS input script for the shock simulation is provided in Supplemental Materials [74] (section SM-3). As these compressive waves reach a free surface, they become tensile in nature and a rarefaction fan propagates back into the sample. This setup was designed to generate a wide range of compressive and tensile states, which sample a wide range of deviatoric stress states, subjecting the mechanophore to various dynamical loads and, hypothetically, inducing many-body intra-molecular strains. A second set of simulations were carried out to explore the response of the system under sustained shock compression. In this setup, the smaller, left slab (projectile) is held perfectly rigid and is impacted in a reverse-ballistic manner by the large slab leading to a single compressive shock. When the shock reaches the free surface at the far end of the target slab, shock absorbing boundary conditions (SABCs) [40,75,76] are applied to keep the system in the compressed state indefinitely. We will refer to this second setup as “sustained shock” and the first one as “shock and spall”. All reactions were determined using ReaxFF bond orders with a cutoff of 0.3 [70,77].

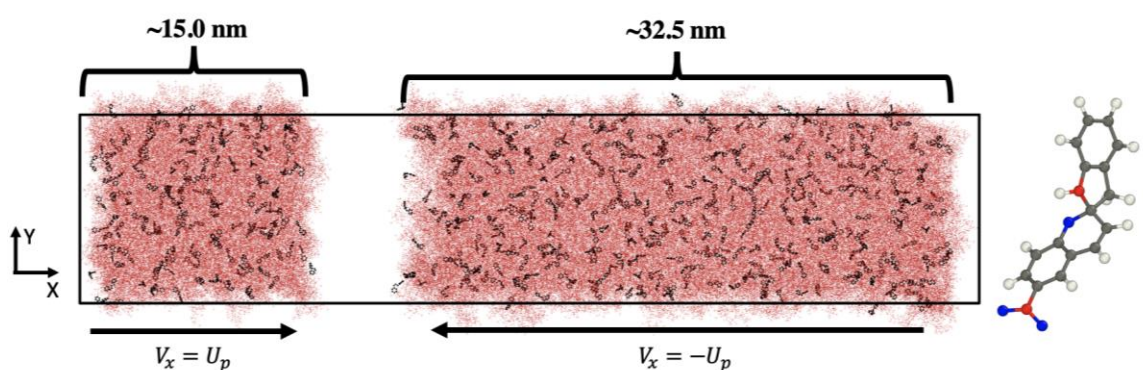


Figure 1: Set-up for shock simulations of the Spiropyran + PMMA system. Atoms colored in red are PMMA backbone carbons, atoms in black are Spiropyran ring atoms. For the 'one-slab' system, the left piece is kept perfectly rigid to approximate an infinitely massive piston.

Results and Discussion

Figure 2 shows x-t diagrams along the shock direction colored by local particle velocity along the shock direction, temperature, and pressure tensor component in the shock direction (P_{xx} , the negative of the stress component σ_{xx}) for the shock & spall system with a u_p of 4 km/s. These diagrams plot, using Eulerian binning, a local property (as the color) a function of position along the shock direction (x) for each time frame (t). The plots show the propagation of the two compressive shockwaves and rarefaction fans after the interaction of the shocks with the free surfaces. The negative-X direction moving wave reaches the free surface just after 2 ps, creating a rarefaction fan that propagates in the positive x direction at a faster velocity than the shock (shock velocity is the inverse of the slope in x-t diagrams). The positive x (rightward) moving shock reaches the other free surface at ~4.5 ps, forming a second rarefaction fan and expanding the material outwards. The two rarefaction waves meet at about 5ps, creating a state of high tensile stress that leads to spall failure. Figure 2 (b) shows that the highest temperature occurs at the impact plane and that the adiabatic cooling upon release/expansion at the free surfaces is on the order of ~200 K. Figures 2 (c) and (d) show P_{xx} at two different scales: the full range of values (panel c from -5 to 35 GPa) and a small range around zero to better see tensile states (panel d from -2 to 2 GPa). Figure 2 (c) shows a shock pressure of about 35 GPa with an almost instantaneous rise. The rarefaction fan forms at the surface, resulting in a nearly instantaneous drop in pressure at the surface, the fan then continuously expands as it propagates across the material. In the last time frame, the fan has expanded such that the pressure drop takes 1.5 ps. Figure 2 d) shows that the rarefaction waves reach tensile stresses of nearly -2 GPa on fast rise times which results in the spall failure of the material and significant extension.

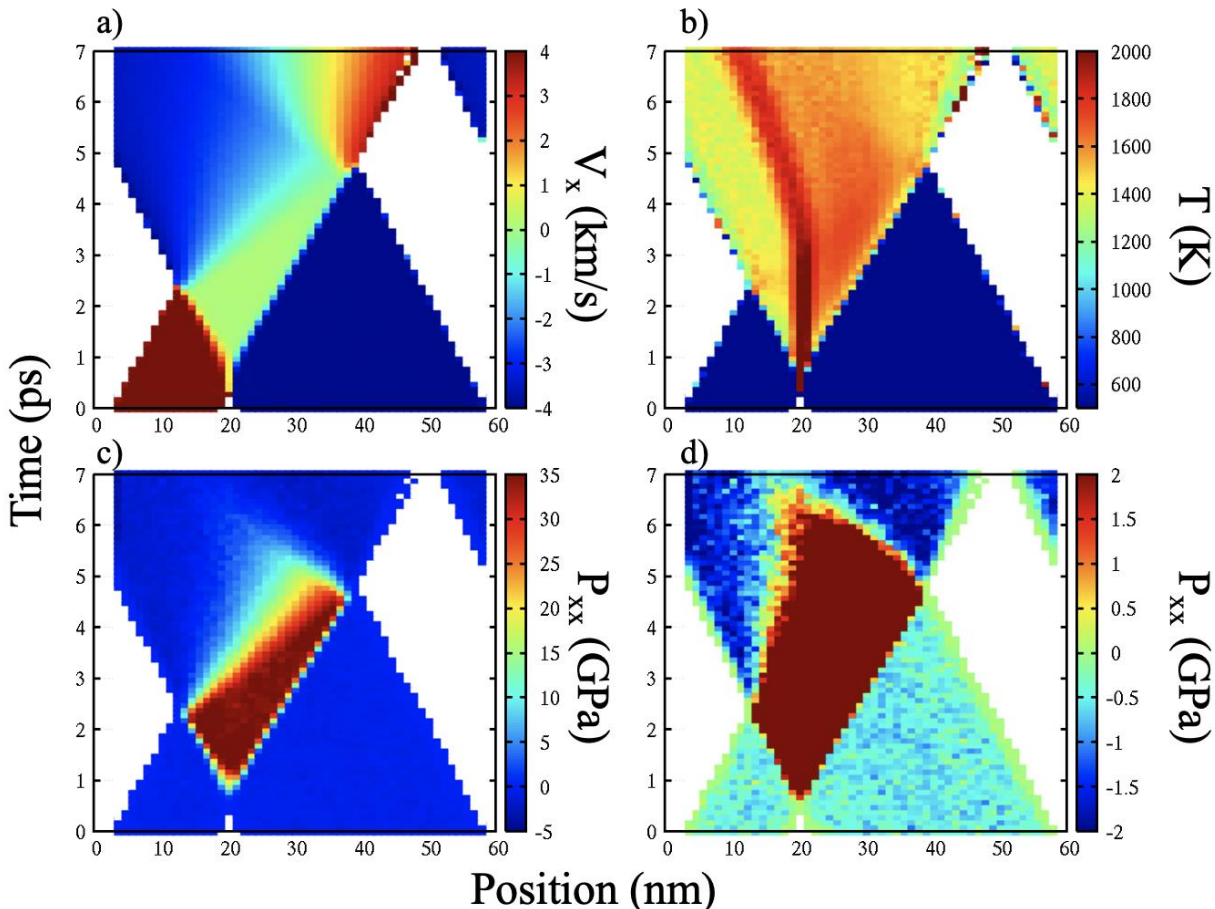


Figure 2: Shock x - t diagrams for $U_p = 4.0$ km/s. Panel a is colored by particle velocity (positive is left to right, or positive x motion), panel b is roto-vibrational temperature, c is pressure and d is pressure with a narrowed color range to better view tensile states.

Previous work has shown the shock compression of molecular solids can lead to significant intra-molecular strain [40,41,78]. The high pressures of the shock state prevent the molecules from conformationally relaxing in a significant way, and this can accelerate chemical reactions [10,48]. To characterize the level of strain of the mechanophores, we track two measures of intra-molecular distortions: i) the distance between the MP anchor atoms that connect the spiropyran with the PMMA on both ends and ii) the torsional dihedral angle around the spiro atom where the C-O breaks during the isomerization reaction; these are shown in Supplemental Materials [74] (section SM-4). The first measure directly tracks the molecular elongation (atomic distance) that is often assumed responsible for inducing the reaction. The second is an intra-molecular rotation that has been traditionally ignored in mechanochemistry studies but has recently been shown to lower the activation barrier of isomerization [48]. Figure 3 shows the distribution of these measures of intramolecular strain under various conditions. These distributions obtained from the geometry of all MPs, 0.2 ps after the passage of the shock front (note that this represents different absolute times for each molecule) are shown as green lines. We determine the shock arrival when the velocity of the molecule reaches within 10% of the expected particle velocity (from the Hugoniot relation) and remains within 10% continuously for 0.5 ps. The red lines correspond to the MPs that reacted during the shock and spall simulation (a subset of the molecular shown in green but at different times). To establish a baseline, these deformations have also been measured

in an equilibrated sample under no mechanical load (300 K, 1 atm), see blue lines in Fig. 3, as well as for a periodic system subjected to uniaxial tensile deformation at a strain rate of $1 \times 10^9/s$, averaged over 1.5% and 2.5% strain (brown lines). Shocked State distributions for different shock pressures are shown in Supplemental Materials [74] (section SM-6).

The uniaxial, uniform strain has little effect on the distributions of each deformation, which is not surprising for a glassy PMMA system that will not undergo significant chain re-alignment on such small strains and short timescales. However, under shock compression, which has been shown to significantly increase chain activity directly behind the shockwave [55], the distributions of molecular deformations are significantly broadened. For the distance between anchor atoms, shock compression naturally leads to significant shortening as compared to the equilibrium distribution, as the spiropyran molecules can fold/rotate around the spiro atom. However, this is not an entirely fair comparison as the maximum compression of the shockwave is $\sim 50\%$ strain. Interestingly, there is also a slight expansion of the distribution towards longer distances, which may be a result of spiropyran monomers oriented normal to the shock direction expanding in the transverse direction during compression, or effects from thermal expansion, or rapid molecular re-alignments [55]. As hypothesized, the compression of the MPs also leads to significant many-body distortions, originating from the rotation around the spiro atom, extending the tail of the dihedral angle distribution by $\sim 50^\circ$. This helps to show that the MPs that react on shock rise and rarefaction timescales are not limited to those with significant intra-molecular strain, but the many-body strain does influence the reactivity, increasing its likelihood, in agreement with previous results in many-body mechanochemistry [48].

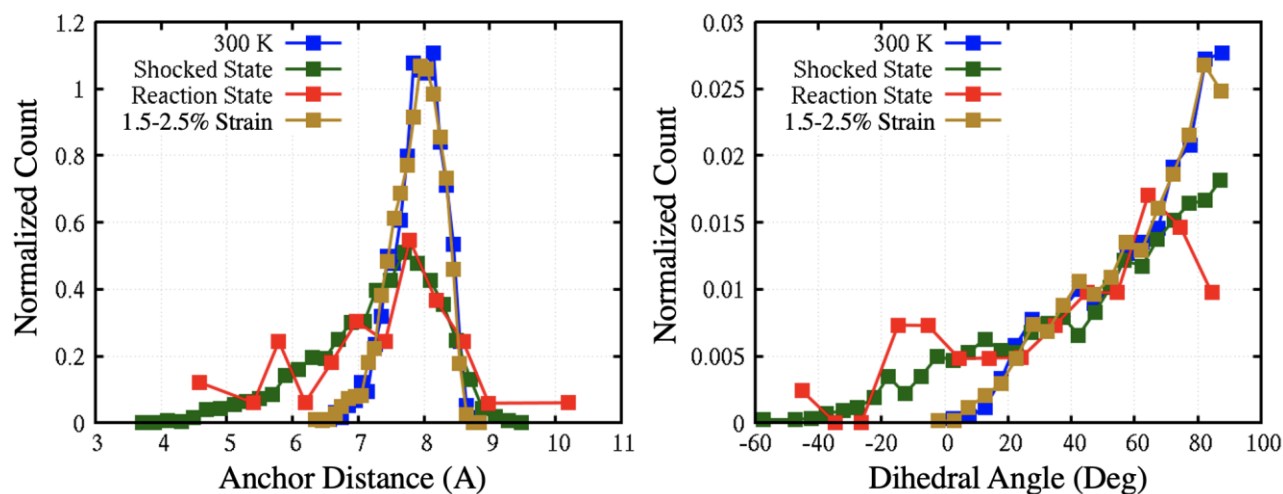


Figure 3: Distributions of spiropyran molecular deformations. Anchor distance is the distance between the two spiropyran carbon atoms bonded to the PMMA backbone carbons for the 4.0 km/s shock. Dihedral angle is the angle formed from a N-C-O-C atoms where the central carbon is the spiro atom and the central bond is the C-O bond that breaks during reaction.

Figure 4 shows a scatter plot of the anchor distances and dihedral angles for all MPs 0.2 ps after loading (black) and those that react (red) in the shock and spall case for 4 km/s, dashed lines indicate the equilibrium values at 300 K. These are the same values represented as distributions in Figure 3. As described above, shock loading results in large molecular strains that are not just compression/elongation on the structure but also many-body in nature. Interestingly, the state of

the MP prior to reaction does not follow the same distribution as the shocked states. While the shocked MPs cast a wide range of states, the states just before reaction (red points) fall within a narrower region. MPs experiencing elongation are more likely to react, this is expected. We note that reactions under tension do not require large many-body strains. However, many reactions also occur under compression. Quite remarkably, a significant fraction of MPs undergoes reaction under compression (small anchor distances) with minimal or no tension along the C-O bond. The overwhelming majority of these reactions occur under larger torsional strain, showing that this is most likely a decoupled mechanism from pulling. The Pearson correlation coefficient between anchor distance and dihedral angle for all MPs is -0.069 indicating negligible correlation between these two measures of molecular strain. However, the correlation coefficient for the reactive states is 0.373 , indicating the need of high torsional distortion for reactions under compression or that tension becomes less critical with increasing torsion, which was previously shown to lower the activation barrier [48].

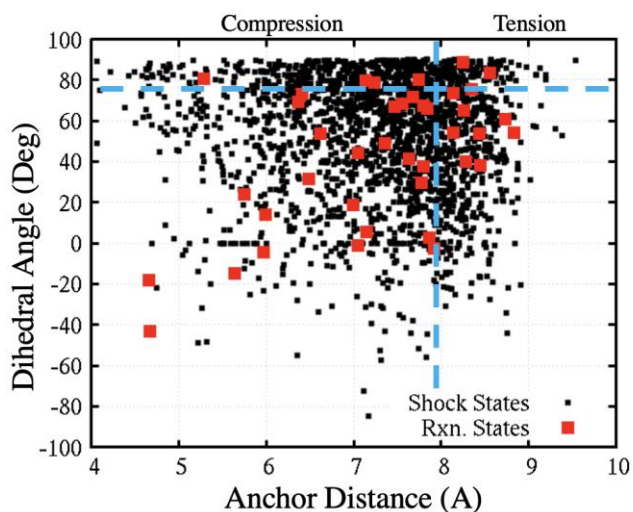


Figure 4: 2D distribution of the deformations shown in Figure 3. Black dots represent shock states and red dots the reacted states. Blue dashed lines are the equilibrium values for each axis.

Figure 5 displays the fraction of MPs that have undergone reaction as a function of simulation time for the shock & spall system (left) and the sustained shock system that only experiences compression (right). This is determined by counting which molecules have a broken C-O bond in each frame, based on ReaxFF bond orders. We plot the total number of activated MPs; a reduction with time indicates reverse reactions. While the conditions in the shock and spall case are experienced over much shorter timescales, relative to the sustained shock, the shock and spall cases show considerably more reactivity, which can be attributed to the presence of tensile stress and the transient states during rarefaction. Decreases in the number of activated MPs most likely stem from the high temperatures of the shocked state inducing the reverse reaction [13,49]. Supplemental Materials [74] (section SM-5) shows versions of these plots with the raw data, not smoothed data, as is shown here.

Focusing on the shock & spall system, the rate of reaction during the early compressive regime shows little to no effect from shock strength except for the weakest shock cases (2.0 and 2.5 km/s). This agrees well with the sustained shock results. However, once the first rarefaction wave forms (2-3 ps), there is a strong dependence of activation rate on the shock strength. This tracks with the

idea that the rarefaction-induced tension and rate of expansion increase with increasing shock strength. The compressive states most likely lead to more many-body intra-molecular strains like the shear induced rotation around the spiro atom, as the higher density restricts spatial relaxations [40], in which the level of intra-molecular strain can play just as much of a role in controlling the reactivity. Since the majority of MPs under shock compression are not experiencing local tensile strains, their reactions are likely dominated by many-body effects. Supplemental Materials [74] (section SM-1) shows that the torsional deformations shown in Figure 3 are not overly influenced by shock strength in the regimes studied here, which agrees well with the trends in reactivity for pure compression. In these cases, the unreacted MPs may be nearing the physical limit of deformations without breaking bonds, meaning that stronger shocks cannot physically push the molecules further. The reactions at later times are driven by tensile stresses which will more directly correspond to shock strength due to the strong relationship of shock strength and the tensile state achieved via rarefaction.

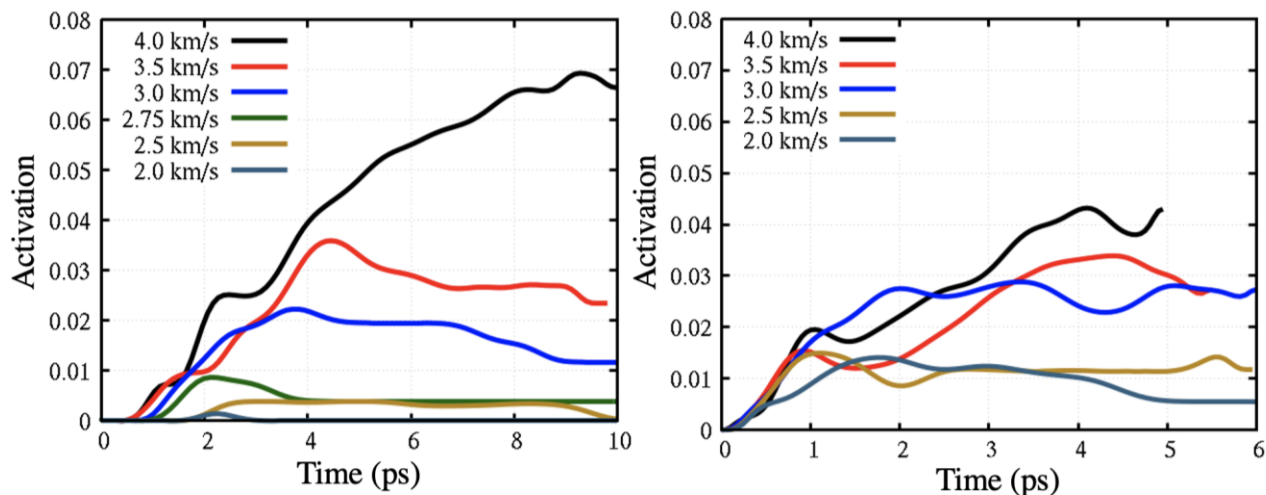


Figure 5: Fraction of spiropyran molecules with broken C-O bonds (at the spiro atom) across time for all impact velocities.

To further investigate the local conditions needed to activate MPs, Figure 6 maps all reactions based on their local pressure and its time-derivative right before reaction, for the shock and spall case with impact velocity of 4.0 km/s. Points are colored by the center of mass velocity of the corresponding MPs in the shock direction. Pressure was determined by averaging the local atomic stresses in a sphere with a radius of 1.5 nm, centered at the spiro atom. Time derivatives of the stress were calculated from 0.3 to 0.1 ps prior to the reaction. The center of mass velocity is not locally averaged and is only based on the atoms in the MP block of the polymer.

Based on the pressure and its time derivative, the reaction states of the MPs can be grouped into four main categories. States with positive pressure time derivative and nonzero pressures are reactions that occur during loading, with the velocity distinguishing the negative X (leftward) or positive X (rightward) moving shock. Reactions at high pressure and near-zero slope occur under compression, following the passage of the shock, and should typically be near zero velocity as well. A few reactions are observed during the unloading process, they correspond to nonzero pressure and negative slopes. While these states experience an expanding system, they have yet to reach a tensile state. The last cluster of reactions corresponds to near-zero slope and negative

pressures, labeled as unloaded and spall. The majority of these states have large, negative particle velocities, meaning that the rarefaction fan has projected the molecules forward in an expansion. Supplemental Materials [74] (section SM-2) zooms in on these states and shows that they have pressures between -1 and -2 GPa.

In summary, the MPs react under a variety of conditions, including compression where chemistry is driven by local shears strains and many-body deformations, during spall/expansion, which is driven by the tensile states, and in the transients in between the two. Roughly half of the reactions occur during transient states, either loading or unloading, in which glassy polymers are known to rapidly evolve under shock loading [55], and the remaining half of the reactions happen under either compression and tension when pressure/strain is more constant. However, due to the relevant length and timescales of both compression and tension, as well as the disparate energy states of the two, it is difficult to resolve a general efficiency of one type of loading against the other.

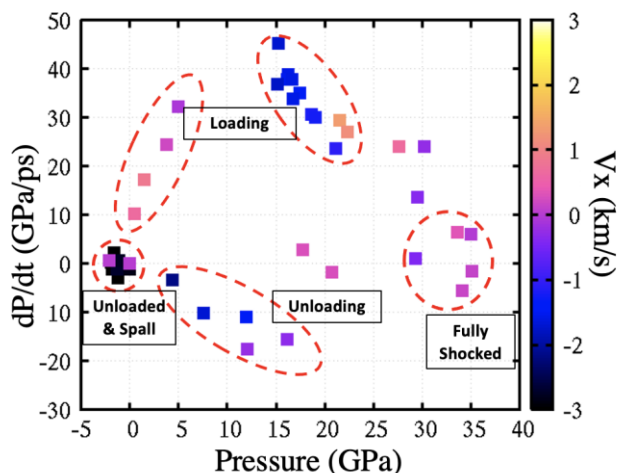


Figure 6: Parametric plot of the pressure and pressure time derivative directly before C-O bond scission for reaction spiropyran in the $U_p = 4.0$ km/s case. Color is velocity in the shock direction, which is zero in the compressed state.

Conclusions

In this work, shock simulations were conducted using an all-atom reactive representation of a PMMA-spiropyran copolymer. The geometry of the system was designed to induce significant compressive stresses and tensile stresses that lead to spall, which would also incur significant resolved shear stresses. These extreme stress states and high strain rates lead to significant intramolecular strain in the mechanophore, which is characterized by the distance between the anchor atoms of the mechanophore (an effective molecular length) and the dihedral angle around the central torsion of the atom, which contains the C-O bond that breaks during isomerization. During rarefaction and spall of the material following a shock with $u_p=4$ km/s, tensile stresses of nearly 2 GPa are reached, while the compressive shock approaches 40 GPa of pressure. Both compression and tension induce significant mechanophore activation, with the tensile/spall activation being much more shock strength-dependent than under compression. The overall reactivity in the systems subjected to compression followed by spall is strongly dependent on shock strength, in

which stronger shocks will lead to both larger compression and larger tensions upon unloading. In the compression only cases, the reactivity does not significantly increase with increasing pressure. This indicates that the compression triggered mechanisms for reactivity may be saturating in the range of shock strengths and timescales studied here. In both cases, we see reactions not only under the elongation of mechanophores, but also driven by torsional distortions where little to no elongation occurs. Lastly, an analysis of the stress-velocity states during activation reveals that mechanochemistry not only occurs during the compressed and strained states, but as well as in the relaxed system, post spall, where the material has begun to fail and does not hold a local stress. These results show the critical need for a better understanding of how deviatoric stress states and intra-molecular strain states can alter condensed matter chemistry, especially that of mechanochemistry. Further work on the effect of strain rates on the activation of condensed phase mechanophores via simulations with uniform tension and compression would be important to quantify rate effects.

Acknowledgments

This work was primarily supported by the US Office of Naval Research, Multidisciplinary University Research Initiatives (MURI) Program, Contract: N00014-16-1-2557. Program managers: Chad Stoltz and Kenny Lipkowitz. We acknowledge computational resources from nanoHUB and Purdue University through the Network for Computational Nanotechnology.

References

- [1] B. W. Hamilton, M. P. Kroonblawd, and A. Strachan, *Extemporaneous Mechanochemistry: Shockwave Induced Ultrafast Chemical Reactions Due to Intramolecular Strain Energy*, *J. Phys. Chem. Lett.* **13**, 6657 (2022).
- [2] J. Ribas-Arino and D. Marx, *Covalent Mechanochemistry: Theoretical Concepts and Computational Tools with Applications to Molecular Nanomechanics*, *Chem. Rev.* **112**, 5412 (2012).
- [3] K. J. Ardila-Fierro and J. G. Hernández, *Sustainability Assessment of Mechanochemistry by Using the Twelve Principles of Green Chemistry*, *ChemSusChem* **14**, 2145 (2021).
- [4] N. Deneke, M. L. Rencheck, and C. S. Davis, *An Engineer's Introduction to Mechanophores*, *Soft Matter* **16**, 6230 (2020).
- [5] M. P. Kroonblawd and N. Goldman, *Mechanochemical Formation of Heterogeneous Diamond Structures during Rapid Uniaxial Compression in Graphite*, *Phys. Rev. B* **97**, 1 (2018).
- [6] M. P. Kroonblawd, R. K. Lindsey, and N. Goldman, *Synthesis of Functionalized Nitrogen-Containing Polycyclic Aromatic Hydrocarbons and Other Prebiotic Compounds in Impacting Glycine Solutions*, *Chem. Sci.* **10**, 6091 (2019).
- [7] Z. Martins, M. C. Price, N. Goldman, M. A. Sephton, and M. J. Burchell, *Shock Synthesis of Amino Acids from Impacting Cometary and Icy Planet Surface Analogues*, *Nat. Geosci.* **6**, 1045 (2013).
- [8] B. A. Steele, N. Goldman, I. F. W. Kuo, and M. P. Kroonblawd, *Mechanochemical Synthesis*

- of Glycine Oligomers in a Virtual Rotational Diamond Anvil Cell*, Chem. Sci. **11**, 7760 (2020).
- [9] M. A. Wood, M. J. Cherukara, E. M. Kober, and A. Strachan, *Ultrafast Chemistry under Nonequilibrium Conditions and the Shock to Deflagration Transition at the Nanoscale*, J. Phys. Chem. C **119**, 22008 (2015).
- [10] M. P. Kroonblawd and L. E. Fried, *High Explosive Ignition through Chemically Activated Nanoscale Shear Bands*, Phys. Rev. Lett. **124**, 206002 (2020).
- [11] C. J. Eckhardt, *Mechanochemistry: The Last Energetic Frontier*, Mol. Cryst. Liq. Cryst. **456**, 1 (2006).
- [12] B. W. Hamilton, M. N. Sakano, C. Li, and A. Strachan, *Chemistry Under Shock Conditions*, Annu. Rev. Mater. Res. **51**, 101 (2021).
- [13] D. A. Davis, A. Hamilton, J. Yang, L. D. Cremar, D. Van Gough, S. L. Potisek, M. T. Ong, P. V. Braun, T. J. Martínez, S. R. White, J. S. Moore, and N. R. Sottos, *Force-Induced Activation of Covalent Bonds in Mechanoresponsive Polymeric Materials*, Nature **459**, 68 (2009).
- [14] M. T. Ong, J. Leiding, H. Tao, A. M. Virshup, and T. J. Martínez, *First Principles Dynamics and Minimum Energy Pathways for Mechanochemical Ring Opening of Cyclobutene*, J. Am. Chem. Soc. **131**, 6377 (2009).
- [15] Y. Chen, A. J. H. Spiering, S. Karthikeyan, G. W. M. Peters, E. W. Meijer, and R. P. Sijbesma, *Mechanically Induced Chemiluminescence from Polymers Incorporating a 1,2-Dioxetane Unit in the Main Chain*, Nat. Chem. **4**, 559 (2012).
- [16] J. Wang, T. B. Kouznetsova, Z. Niu, M. T. Ong, H. M. Klukovich, A. L. Rheingold, T. J. Martinez, and S. L. Craig, *Inducing and Quantifying Forbidden Reactivity with Single-Molecule Polymer Mechanochemistry*, Nat. Chem. **7**, 323 (2015).
- [17] P. Cai, B. Hu, W. R. Leow, X. Wang, X. J. Loh, Y. L. Wu, and X. Chen, *Biomechano-Interactive Materials and Interfaces*, Adv. Mater. **30**, (2018).
- [18] K. Joshi, M. Scheiner, D. O. Olawale, and T. J. Dickens, *Triboluminescent Sensors for Polymer-Based Composites*, in *Triboluminescence* (Springer, 2016), pp. 305–332.
- [19] M. A. S. Shohag, S. A. Tran, T. Ndebele, N. Adhikari, and O. I. Okoli, *Designing and Implementation of Triboluminescent Materials for Real-Time Load Monitoring*, Mater. Des. **153**, 86 (2018).
- [20] A. Piermattei, S. Karthikeyan, and R. P. Sijbesma, *Activating Catalysts with Mechanical Force*, Nat. Chem. **1**, 133 (2009).
- [21] A. L. B. Ramirez, Z. S. Kean, J. A. Orlicki, M. Champhekar, S. M. Elsagr, W. E. Krause, and S. L. Craig, *Mechanochemical Strengthening of a Synthetic Polymer in Response to Typically Destructive Shear Forces*, Nat. Chem. **5**, 757 (2013).
- [22] X. Hu, T. Zeng, C. C. Husic, and M. J. Robb, *Mechanically Triggered Small Molecule Release from a Masked Furfuryl Carbonate*, J. Am. Chem. Soc. **141**, 15018 (2019).
- [23] M. Grandbois, M. Beyer, M. Rief, H. Clausen-Schaumann, and H. E. Gaub, *How Strong Is a Covalent Bond?*, Science (80-.). **283**, 1727 (1999).
- [24] T. Stauch and A. Dreuw, *Advances in Quantum Mechanochemistry: Electronic Structure Methods and Force Analysis*, Chem. Rev. **116**, 14137 (2016).
- [25] Z. Huang, Q. Z. Yang, D. Khvostichenko, T. J. Kucharski, J. Chen, and R. Boulatov, *Method to Derive Restoring Forces of Strained Molecules from Kinetic Measurements*, J. Am.

- Chem. Soc. **131**, 1407 (2009).
- [26] T. Stauch and A. Dreuw, *Knots “Choke Off” Polymers upon Stretching*, *Angew. Chemie - Int. Ed.* **55**, 811 (2016).
- [27] A. M. Saitta and M. L. Klein, *Evolution of Fragments Formed at the Rupture of a Knotted Alkane Molecule*, *J. Am. Chem. Soc.* **121**, 11827 (1999).
- [28] A. M. Saitta, P. D. Soper, E. Wasserman, and M. L. Klein, *Influence of a Knot on the Stength of a Polymer Strand*, *Nature* **399**, 46 (2019).
- [29] M. L. Mansfield, *Knots in Hamilton Cycles*, *Macromolecules* **27**, 5924 (1994).
- [30] M. Paulsson, C. Krag, T. Frederiksen, and M. Brandbyge, *Conductance of Alkanedithiol Single-Molecule Junctions: A Molecular Dynamics Study*, *Nano Lett.* **9**, 117 (2009).
- [31] Y. Qi, J. Qin, G. Zhang, and T. Zhang, *Breaking Mechanism of Single Molecular Junctions Formed by Octanedithiol Molecules and Au Electrodes*, *J. Am. Chem. Soc.* **131**, 16418 (2009).
- [32] P. Vélez, S. A. Dassie, and E. P. M. Leiva, *First Principles Calculations of Mechanical Properties of 4,4'-Bipyridine Attached to Au Nanowires*, *Phys. Rev. Lett.* **95**, 2 (2005).
- [33] T. Stauch, M. T. Hoffmann, and A. Dreuw, *Spectroscopic Monitoring of Mechanical Forces during Protein Folding by Using Molecular Force Probes*, *ChemPhysChem* **17**, 1486 (2016).
- [34] C. Jarzynski, *Nonequilibrium Equality for Free Energy Differences*, *Phys. Rev. Lett.* **78**, 2690 (1997).
- [35] C. Jarzynski, *Equilibrium Free-Energy Differences from Nonequilibrium Measurements: A Master-Equation Approach*, *Phys. Rev. E* **56**, 5018 (1997).
- [36] S. Park and K. Schulten, *Calculating Potentials of Mean Force from Steered Molecular Dynamics Simulations*, *J. Chem. Phys.* **120**, 5946 (2004).
- [37] S. Park, F. Khalili-Araghi, E. Tajkhorshid, and K. Schulten, *Free Energy Calculation from Steered Molecular Dynamics Simulations Using Jarzynski’s Equality*, *J. Chem. Phys.* **119**, 3559 (2003).
- [38] B. Isralewitz, M. Gao, and K. Schulten, *Steered Molecular Dynamics and Mechanical Functions of Proteins*, *Curr. Opin. Struct. Biol.* **11**, 224 (2001).
- [39] M. K. Beyer, *The Mechanical Strength of a Covalent Bond Calculated by Density Functional Theory*, *J. Chem. Phys.* **112**, 7307 (2000).
- [40] B. W. Hamilton, M. P. Kroonblawd, C. Li, and A. Strachan, *A Hotspot’s Better Half: Non-Equilibrium Intra-Molecular Strain in Shock Physics*, *J. Phys. Chem. Lett.* **12**, 2756 (2021).
- [41] B. W. Hamilton, M. P. Kroonblawd, and A. Strachan, *The Potential Energy Hotspot: Effects of Impact Velocity, Defect Geometry, and Crystallographic Orientation*, *J. Phys. Chem. C* (2022).
- [42] B. W. Hamilton and T. C. Germann, *Energy Localization Efficiency in 1,3,5-Trinitro-2,4,6-Triaminobenzene Pore Collapse Mechanisms*, *J. Appl. Phys.* **133**, 035901 (2023).
- [43] M. R. Manaa, *Shear-Induced Metallization of Triamino-Trinitrobenzene Crystals*, *Appl. Phys. Lett.* **83**, 1352 (2003).
- [44] E. J. Reed, M. R. Manaa, L. E. Fried, K. R. Glaesemann, and J. D. Joannopoulos, *A Transient Semimetallic Layer in Detonating Nitromethane*, *Nat. Phys.* **4**, 72 (2008).
- [45] A. P. Wiita, S. R. K. Ainaravapu, H. H. Huang, and J. M. Fernandez, *Force-Dependent Chemical Kinetics of Disulfide Bond Reduction Observed with Single-Molecule Techniques*,

- Proc. Natl. Acad. Sci. U. S. A. **103**, 7222 (2006).
- [46] V. V. Rybkin, *Franck-Condon Theory of Quantum Mechanochemistry*, J. Phys. Chem. A **121**, 5758 (2017).
- [47] G. I. Bell, *Models for the Specific Adhesion of Cells to Cells*, Science (80-.). **200**, 618 (1978).
- [48] B. W. Hamilton and A. Strachan, *Many-Body Mechanochemistry : Intra-Molecular Strain in Condensed Matter Chemistry*, ChemRxiv (2022).
- [49] J. W. Kim, Y. Jung, G. W. Coates, and M. N. Silberstein, *Mechanoactivation of Spiropyran Covalently Linked Pmma: Effect of Temperature, Strain Rate, and Deformation Mode*, Macromolecules **48**, 1335 (2015).
- [50] C. K. Lee, D. A. Davis, S. R. White, J. S. Moore, N. R. Sottos, and P. V. Braun, *Force-Induced Redistribution of a Chemical Equilibrium*, J. Am. Chem. Soc. **132**, 16107 (2010).
- [51] C. M. Kingsbury, P. A. May, D. A. Davis, S. R. White, J. S. Moore, and N. R. Sottos, *Shear Activation of Mechanophore-Crosslinked Polymers*, J. Mater. Chem. **21**, 8381 (2011).
- [52] G. R. Gossweiler, T. B. Kouznetsova, and S. L. Craig, *Force-Rate Characterization of Two Spiropyran-Based Molecular Force Probes*, J. Am. Chem. Soc. **137**, 6148 (2015).
- [53] M. B. Larsen and A. J. Boydston, *"Flex-Activated" Mechanophores: Using Polymer Mechanochemistry to Direct Bond Bending Activation*, J. Am. Chem. Soc. **135**, 8189 (2013).
- [54] B. A. Beiermann, S. L. Kramer, P. A. May, J. S. Moore, S. R. White, and N. R. Sottos, *The Effect of Polymer Chain Alignment and Relaxation on Force-induced Chemical Reactions in an Elastomer.*, Adv. Funct. Mater. **24**, 1529 (2014).
- [55] J. Macatangay, B. W. Hamilton, and A. Strachan, *Deviatoric Stress Driven Transient Melting Below the Glass Transition Temperature in Shocked Polymers*, J. Appl. Phys. **132**, (2022).
- [56] S. Plimpton, *Fast Parallel Algorithms for Short-Range Molecular Dynamics*, J. Comput. Phys. **117**, 1 (1995).
- [57] L. Liu, Y. Liu, S. V. Zybin, H. Sun, and W. A. Goddard, *ReaxFF-Lg: Correction of the ReaxFF Reactive Force Field for London Dispersion, with Applications to the Equations of State for Energetic Materials*, J. Phys. Chem. A **115**, 11016 (2011).
- [58] G. M. Odegard, B. D. Jensen, S. Gowtham, J. Wu, J. He, and Z. Zhang, *Predicting Mechanical Response of Crosslinked Epoxy Using ReaxFF*, Chem. Phys. Lett. **591**, 175 (2014).
- [59] C. de Tomas, I. Suarez-Martinez, and N. A. Marks, *Graphitization of Amorphous Carbons: A Comparative Study of Interatomic Potentials*, Carbon N. Y. **109**, 681 (2016).
- [60] B. W. Hamilton, B. A. Steele, M. N. Sakano, M. P. Kroonblawd, I. F. W. Kuo, and A. Strachan, *Predicted Reaction Mechanisms, Product Speciation, Kinetics, and Detonation Properties of the Insensitive Explosive 2,6-Diamino-3,5-Dinitropyrazine-1-Oxide (LLM-105)*, J. Phys. Chem. A **125**, 1766 (2021).
- [61] B. W. Hamilton, M. P. Kroonblawd, M. M. Islam, and A. Strachan, *Sensitivity of the Shock Initiation Threshold of 1,3,5-Triamino-2,4,6-Trinitrobenzene (TATB) to Nuclear Quantum Effects*, J. Phys. Chem. C **123**, 21969 (2019).
- [62] B. P. Haley, N. Wilson, C. Li, A. Arguelles, E. Jaramillo, and A. Strachan, *Atomistic Simulations of Amorphous Polymers in the Cloud with PolymerModeler*, ArXiv:

- 1503.03894 (2015).
- [63] J. Ilja Siepmann and D. Frenkel, *Configurational Bias Monte Carlo: A New Sampling Scheme for Flexible Chains*, *Mol. Phys.* **75**, 59 (1992).
- [64] S. L. Mayo, B. D. Olafson, and W. A. Goddard, *DREIDING: A Generic Force Field for Molecular Simulations*, *J. Phys. Chem.* **94**, 8897 (1990).
- [65] L. Alzate-Vargas, N. Onofrio, and A. Strachan, *Universality in Spatio-Temporal High-Mobility Domains across the Glass Transition from Bulk Polymers to Single Chains*, *Macromolecules* **53**, 9375 (2020).
- [66] S. V. Zybin, W. A. Goddard, P. Xu, A. C. T. Van Duin, and A. P. Thompson, *Physical Mechanism of Anisotropic Sensitivity in Pentaerythritol Tetranitrate from Compressive-Shear Reaction Dynamics Simulations*, *Appl. Phys. Lett.* **96**, 1 (2010).
- [67] L. Zhang, S. V Zybin, A. C. T. Van Duin, S. Dasgupta, W. A. G. Iii, and E. M. Kober, *High Explosives from ReaxFF Reactive Molecular Dynamics Simulations*, Society 10619 (2009).
- [68] M. A. Wood, D. E. Kittell, C. D. Yarrington, and A. P. Thompson, *Multiscale Modeling of Shock Wave Localization in Porous Energetic Material*, *Phys. Rev. B* **97**, 1 (2018).
- [69] T. R. Shan, R. R. Wixom, and A. P. Thompson, *Extended Asymmetric Hot Region Formation Due to Shockwave Interactions Following Void Collapse in Shocked High Explosive*, *Phys. Rev. B* **94**, (2016).
- [70] T. P. Senftle, S. Hong, M. M. Islam, S. B. Kylasa, Y. Zheng, Y. K. Shin, C. Junkermeier, R. Engel-Herbert, M. J. Janik, H. M. Aktulga, T. Verstraelen, A. Grama, and A. C. T. Van Duin, *The ReaxFF Reactive Force-Field: Development, Applications and Future Directions*, *Npj Comput. Mater.* **2**, (2016).
- [71] D. Guo, Q. An, W. A. Goddard, S. V. Zybin, and F. Huang, *Compressive Shear Reactive Molecular Dynamics Studies Indicating That Cocrystals of TNT/CL-20 Decrease Sensitivity*, *J. Phys. Chem. C* **118**, 30202 (2014).
- [72] M. S. Powell, M. N. Sakano, M. J. Cawkwell, P. R. Bowlan, K. E. Brown, C. A. Bolme, D. S. Moore, S. F. Son, A. Strachan, and S. D. McGrane, *Insight into the Chemistry of PETN under Shock Compression through Ultrafast Broadband Mid-Infrared Absorption Spectroscopy*, *J. Phys. Chem. A* **124**, 7031 (2020).
- [73] B. L. Holian and G. K. Straub, *Molecular Dynamics of Shock Waves in Three-Dimensional Solids: Transition from Nonsteady to Steady Waves in Perfect Crystals and Implications for the Rankine-Hugoniot Conditions*, *Phys. Rev. Lett.* **43**, 1598 (1979).
- [74] *See Supplemental Materials at [Link].*
- [75] M. J. Cawkwell, T. D. Sewell, L. Zheng, and D. L. Thompson, *Shock-Induced Shear Bands in an Energetic Molecular Crystal: Application of Shock-Front Absorbing Boundary Conditions to Molecular Dynamics Simulations*, *Phys. Rev. B - Condens. Matter Mater. Phys.* **78**, 1 (2008).
- [76] S. Zhao, T. C. Germann, and A. Strachan, *Molecular Dynamics Simulation of Dynamical Response of Perfect and Porous NiAl Nanolaminates under Shock Loading*, *Phys. Rev. B - Condens. Matter Mater. Phys.* **76**, 1 (2007).
- [77] A. C. T. Van Duin, S. Dasgupta, F. Lorant, and W. A. Goddard, *ReaxFF: A Reactive Force Field for Hydrocarbons*, *J. Phys. Chem. A* **105**, 9396 (2001).
- [78] M. P. Kroonblawd, B. A. Steele, M. D. Nelms, L. E. Fried, and R. A. Austin, *Anisotropic Strength Behavior of Single-Crystal TATB*, *Model. Simul. Mater. Sci. Eng.* **30**, 014004

(2021).